EXTENDED EXPERIMENTAL PROCEDURES

Kinase Translocation Reporter (KTR) technology is based on the fact that a phosphate group can modulate the affinity by which nuclear localization signals (NLS) and nuclear export signals (NES) bind to importins and exportins. Although multiple arrangements might lead to this effect, here we discuss how NLS, NES and phosphorylation sites are engineered in our approach and how the sequence context influences the final outcome. Amino acids are named using the one letter code. This explanation is based on data shown in Figures 1C and S2D–S2F.

Export

Nuclear export signals are usually defined by 4 hydrophobic amino acids with conserved spacing (Wen et al., 1995). This spacing has been used to classify NESs into 3 main groups (Kosugi et al., 2008). Traditionally, the most widely observed NES is: $\Phi X_1 X_2 X_3 \Phi X_4 X_5 \Phi X_6 \Phi$ (Φ is a hydrophobic amino acid). Usually the hydrophobic amino acids are L and occasionally I, V, M or F. However, previous studies have shown that one of the four key amino acids can be substituted by W, C, T or A (Kosugi et al., 2008). The NES found in c-Jun is …ASPELERLII… Nuclear export activities are determined by the sequence and its context thus, the more we differ from the consensus sequence the worse the export rate will be. c-Jun NES sequence has a low export rate for many reasons, one of which is that hydrophobic amino acids in the spacing regions have been shown to diminish the export rate (Kosugi et al., 2008) and there is an I at position X_6. Another is that the first hydrophobic amino acid is an A, which is not one of the consensus amino acids. Therefore, the first sequence variants that we included in our screen were designed to increase the export rate of the endogenous c-Jun sequence (compare WT to E1 and E3 sequences). Indeed, the dynamic range increased in both E1 and E3. More importantly, however, the basal localization shifted to be more cytoplasmic. In fact, the E3 sequence was too cytoplasmic, such that the dynamic range was not as good as that of E1. This result indicates that the export rate should be suboptimal so that phosphorylation causes a maximal change in localization.

We also explored how increasing putative phosphorylation sites might increase the dynamic range. Variants E3 to E6 vary in the amount of putative SP sites. Adding an SP site at positions X_4 X_5 reduced the basal export activity (compare E1 to E2, E3 to E4 or E5 to E6). This result has two main explanations: the presence of a proline and the removal of the negative charge. The presence of a proline at X_5 position alters the basal export rate of the NES (compare E13 with E14 and see Kosugi et al. [2008]). In fact, P anywhere inside the export signal tends to reduce its activity (compare E7 to E8, E16 to E18 and E11 to E12). Therefore, exploring how increasing phosphorylation sites modulate the dynamic range is difficult because JNK is a proline directed kinase. This means that the combined effect of the P inside the export sequence and the S being phosphorylated will partially compensate. To prevent proline from being inside the export sequence (reducing its activity) we added …VSSR… as the first four amino acids on the NES (E7) (based on the DNA helicase B phospho-regulated sequence [Hahn et al., 2009]). Accordingly, this sequence had the highest basal export activity. Interestingly, we found that phosphorylation upstream of the NES also induces an increase on export rate, although E7 did not have the highest dynamic range (compare with E16). The removal of the negative charge present in an export sequence reduces export rate (compare E7 to E16). Taking all of these findings together, we concluded that the generation of phosphorylation-enhanced nuclear export requires the presence of negative charges to increase export rate. A clear example is shown by comparing E7 to E16 and to E15. These sequences differ in the amount of negative charge (E7 > E16 > E15), which correlate with basal cytoplasmic localization (E7 > E16 > E15). Interestingly, phosphorylation increases the export rate of all these constructs, indicating that the more negative charges, the more efficient export is. That E16 has the higher dynamic range underlines the idea of a balance between how active the export sequence is and whether an extra charge will induce a maximal effect.

Import

In order to increase the dynamic range of our synthetic kinase activity reporter, we decided to include a negatively regulated import sequence. Nuclear localization signals (NLS) are often defined as a sequence enriched in basic amino acids (K or R) (Kosugi et al., 2009). Among several examples found in the literature (Nardozzi et al., 2010), DNA helicase B (Hahn et al., 2009) was the one that we focused on understanding. In general, none of the examples matched a consensus NLS sequence, highlighting that import sequence activity, similarly to export, needs to be suboptimal for the phosphorylation to induce a maximal change. We found that DNA helicase B has a phosphorylation site in what appears to be a non-consensus bipartite NLS. Bipartite NLS (bNLS) consensus sequences are defined as $KRX_{10\text{-}12}K(K/R)(K/R)$, and acidic residues should be rich in the central region of the linker but rare in the terminal linker region(Kosugi et al., 2009). In fact, DNA helicase B bNLS sequence is …KRTCGVNDDE**S**PSKIF… This sequence matches the description of a bNLS without the last 2 basic amino acids. Interestingly, the phosphorylation occurs at the terminal region of the linker, where acidic amino acids should be rare. We speculated that a phosphorylation in this position might reduce the import activity of the sequence. Therefore, we generated c-Jun sequence variants to convert the S63 phosphorylation site into a regulated bipartite NLS. Importantly, JNK should still be able to phosphorylate this site.

Based on the above, we divided the bipartite NLS as follows: KR-Linker-(K_x). The linker region is in turn divided in initial, central and terminal linker regions. Adding the two basic amino acid segments of a consensus bNLS sequence in the c-Jun S63 context works as an NLS but is hardly regulated by phosphorylation (I10). As in the NES sequence, removing the two acid amino acids from the linker region increased the import activity under basal conditions (compare I10 to I11) indicating that acidic amino acids in the initial or terminal linker regions reduce bNLS activity. This was the key finding that allows converting phosphorylation (which introduces negative

charges) into changes in import rates. However, in this case (I1, I10 and I11), there is no clear increase on the dynamic range, probably because the phosphorylation occurs in the central part of the linker, where charges are supposed to have a positive effect on the import rate. I3 to I6 variants have the phosphorylation sites in the terminal linker region and these variants showed a substantial increase in dynamic range. The two key features for our optimal phospho-regulated import sequence (I7) are: the number of basic amino acids in the second segment of basic amino acids (compare I6 to I7 and I12 to I15) and the complete absence of acidic amino acids in the terminal linker region (compare I7 to I8). The initial and central linker regions can be variable, with some differences in dynamic range (compare I7 to I12, I13 or I14). Importantly, the acidic central linker region can eventually be replaced by other amino acids, but at the cost of nuclear import rate (compare I7 to I13). Finally, phosphorylation can also occur in the initial linker region with the same or even better dynamic range (compare I7 to I16). Taken together, these results indicate that a positive charge balance (acidic or phosphorylation versus basic amino acids) at either end of the bNLS regulates its import activity, most likely by securing its interaction with importins.

Combining Import and Export

With a clear candidate for phospho-regulated bNLS (I7), we tried several combinations of I7 with different phospho-regulated NES. Interestingly, in most cases, the combinations were not additive. One possible explanation for this is that neither import nor export is completely off in the phosphorylated or unphosphorylated state respectively. Therefore, a balance between residual and full activities must exist. Comparing C3 and C4 is a clear example. Both variants have the same NLS sequence, but the NES sequences are different (E7 and E16 respectively). E16 had a larger dynamic range than E7, but when combined with I7 bNLS, E7 is clearly better. Most likely, this is because E7 has a higher export rate (in both phosphorylated and unphosphorylated states) that can overcome the residual import activity from the phosphorylated bNLS sequence. These findings indicate that in order to implement KTR technology for other kinases, the selection of import and export sequences should be considered together.

Construction of Synthetic KTRs

The findings mentioned above are important to understand what the relation between bNLS, NES and phosphorylation sites should be in order to obtain a good dynamic range. However, the second key consideration is how can we achieve kinase specificity. Obviously this depends on each type of kinase. We have investigated kinases with two different mechanisms of specificity, MAP Kinases and AGC kinases. MAP kinases require distant docking sites but have fewer requirements in the context of the phosphorylation site than AGC kinases (Ubersax and Ferrell, 2007). In any case, the design for any kinase requires the sequence of known substrate as a starting point. Accordingly, for MAP kinases, cloning a specific distant docking site was enough to change the specificity of the reporter. ERK KTR also required adjusting the context of the phosphorylation site to ERK's requirements (i.e., P at −2). For AGC kinases the approach was to mutate the context of a naturally occurring phosphorylation site (i.e., HDAC8 for PKA) to introduce a bNLS and a NES without altering the key residues for specificity. Although the sequence space is more limited for this type of kinases, there is still enough flexibility to have all requirements coexisting. The phospho sites can occur at both ends of the bNLS linker which has 10-12 "free" amino acids; for the NES, phosphorylation can happen upstream of the NES with the same effect offering a "free" region to introduce kinase requirements.

Rule Summary

1. bNLS should have 2 basic amino acids followed by a 10-12 amino acid linker and 1-2 more basic amino acids at the end.
2. Phosphorylations should occur close to the basic amino acids to disrupt import rate.
3. 5-10 amino acids downstream a NES should start with the format ΦXXXΦXXΦXΦ (Φ hydrophobic).
4. Phosphorylations should occur upstream of the NES or in the first linker of 3 amino acids to enhance export rate.
5. Certain combinations of basic and hydrophobic aminoacids are better regulated than others (see consensus for our best candidate). In general KR-$X_{10\text{-}12}$-KKK and LXXXLXXLXL should be avoided, as they are too strong to be regulated.
6. Different combinations of bNLS and NES will impact the basal localization of the reporter, but there will always be constant shuttling.
7. Consensus: KR-<u>XXX</u>XXXXXXXX<u>XXX</u>-KK-XX<u>XXX</u>-V-<u>XXX</u>-L-XX-L-X-L. Phospho sites in the underlined regions.

Supplemental Equations

To better understand the quantitative relationship between kinase activity and KTR localization, we developed a mathematical model of the KTR system. The input to the model is the time-course of active kinase concentration, and so the model can also be used in a plug-and-play manner with mathematical models of kinase signaling. In addition, by making certain assumptions, one can go in the reverse direction, to determine the kinase dynamics that could have produced the observed KTR dynamics. Here we describe the construction and underlying assumptions of the model, as well as how we parameterized it for the JNK KTR.

Model Description

Our model of the KTR system consists of ordinary differential equations describing the phosphorylation, dephosphorylation, and nuclear-cytosolic shuttling of the KTR. The model has two compartments: cytosol and nucleus. We also assume that the two phospho-sites of the reporter are either both phosphorylated or both unphosphorylated. Thus, the reporter has four states in the model: unphosphorylated in the cytosol, unphosphorylated in the nucleus, phosphorylated in the cytosol, and phosphorylated in

the nucleus (Figure 4A). The reporter is neither produced nor degraded in the model, so the total concentration of reporter is a parameter.

The key to the KTR system is that the unphosphorylated and phosphorylated versions of the reporter have distinct nuclear import and export rate constants. In particular, the phosphorylated version has a higher export rate constant and a lower import rate constant than the unphosphorylated version. As a result, unphosphorylated reporter is primarily nuclear, whereas phosphorylated reporter is predominantly cytosolic. We model import and export as first order, non-saturating processes.

We model the interaction between kinase and KTR according to Briggs-Haldane kinetics. Here, the parameters are a catalytic rate constant and a Michaelis constant. Importantly, the model does not explicitly represent complexing of the kinase with the reporter. Consequently, the input to the model is a time-course of active kinase concentration in cytosol and in nucleus. This approach results in a straightforward model that matches our experimental data. Additionally, this decoupling of kinase dynamics from KTR dynamics allows one to use the output from any mathematical model of the kinase signaling pathway of interest as input to the model of the respective KTR.

The classic derivation of Briggs-Haldane kinetics requires two assumptions: the quasi-steady-state approximation and the free ligand approximation. Theoretical work by Segel and Slemrod (Segel and Slemrod, 1989) has shown that the Briggs-Haldane analysis is valid if

$$\frac{E_0}{K_m + S_0} \ll 1$$

where E_0 is the initial concentration of enzyme, K_m is the Michaelis constant, and S_0 is the initial concentration of substrate. Given our best estimates of the parameter values for JNK and the reporter (discussed below), we believe the above inequality holds for our system. In addition, empirically, the presence of the reporter does not alter the phosphorylation dynamics of Jun (a substrate of JNK), so the reporter does not seem to be acting as a sink for JNK activity (Figures S2A and S2B). Based on our characterization of several KTRs, we believe that modeling phosphorylation of the reporter according to Briggs-Haldane kinetics will be generally sufficient.

Dephosphorylation of the reporter is also modeled according to Briggs-Haldane kinetics, which means the dephosphorylation rate can saturate. We found that a non-saturating (first order) dephosphorylation term did not fit our experimental data as well. The dephosphorylation term has two parameters, a maximum dephosphorylation rate (V_{max}) and a concentration of reporter for which the dephosphorylation rate is half the maximum (Michaelis constant). The concentration and activity of phosphatase(s) is assumed to be constant during our experiments, and is lumped into the maximum dephosphorylation rate. The model allows different maximum dephosphorylation rates in cytosol and nucleus, but these are very difficult to constrain independently, so we set them equal to each other.

Model Equations and Parameters

$$\frac{dr_{cu}}{dt} = -kin_c(t) \cdot k_{cat} \cdot \frac{r_{cu}}{r_{cu} + K_m} + k_{dc} \cdot \frac{r_{cp}}{r_{cp} + K_{md}} - k_{iu} \cdot r_{cu} + k_{eu} \cdot r_{nu}$$

$$\frac{dr_{nu}}{dt} = -kin_n(t) \cdot k_{cat} \cdot \frac{r_{nu}}{r_{nu} + K_m} + k_{dn} \cdot \frac{r_{np}}{r_{np} + K_{md}} + k_v \cdot k_{iu} \cdot r_{cu} - k_v \cdot k_{eu} \cdot r_{nu}$$

$$\frac{dr_{cp}}{dt} = kin_c(t) \cdot k_{cat} \cdot \frac{r_{cu}}{r_{cu} + K_m} - k_{dc} \cdot \frac{r_{cp}}{r_{cp} + K_{md}} - k_{ip} \cdot r_{cp} + k_{ep} \cdot r_{np}$$

$$\frac{dr_{np}}{dt} = kin_n(t) \cdot k_{cat} \cdot \frac{r_{nu}}{r_{nu} + K_m} - k_{dn} \cdot \frac{r_{np}}{r_{np} + K_{md}} + k_v \cdot k_{ip} \cdot r_{cp} - k_v \cdot k_{ep} \cdot r_{np}$$

$$r_{cu} + r_{cp} + \frac{1}{k_v}(r_{nu} + r_{np}) = r_{total}$$

Symbol Description Estimated value for JNK KTR r_{total} (r_{cu}, r_{nu}, r_{cp}, r_{np}) total reporter concentration (cytosolic or nuclear, unphosphorylated or phosphorylated)0.4 μM (r_{total})k_v ratio of cytosolic volume to nuclear volume4 k_{iu} nuclear import of unphosphorylated reporter0.44 /min k_{eu} nuclear export of unphosphorylated reporter0.11 /min k_{ip} nuclear import of phosphorylated reporter0.16 /min k_{ep} nuclear export of phosphorylated reporter0.2 /min k_{cat} catalytic rate constant of kinase and reporter20 /min K_m Michaelis constant for kinase and reporter3 μM k_{dc} dephosphorylation V_{max} of reporter in cytosol0.03 μM/min k_{dn} dephosphorylation V_{max} of reporter in nucleus0.03 μM /min K_{md} Michaelis constant for dephosphorylation of reporter0.1 μM $kin_c(t)$, $kin_n(t)$ time-dependent concentrations of active kinase in cytosol and nucleus varies.

Sources of Parameter Values

r_{total} – The total concentration of reporter affects the behavior of the system in primarily two ways, through the quantities r_{total}/K_m and r_{total}/K_{md}. These quantities describe the saturation of the kinase and phosphatase for the reporter. Our estimate of r_{total} is informed by a couple pieces of data. First, based on Western blots of the initial version of the JNK reporter, which can be recognized by Jun antibody, we estimate that the concentration of reporter is no more than five times the concentration of Jun (Figure S2A). Second, the response of the JNK KTR (in terms of both phosphorylation and translocation) is just as fast as Jun phosphorylation (Figures S2B and S3D). If [Jun]< $K_m < r_{total}$, we would expect the C/N ratio of the JNK KTR to lag behind Jun phosphorylation. This suggests that the concentrations of reporter and Jun are either both less than K_m or both greater than K_m. We know of no direct measurements of Jun concentration. However, these data together with the low concentrations of similar signaling components and transcription factors in NIH 3T3 cells (Schwanhäusser et al., 2011) and the relatively high Km that has been measured for JNK with Jun (see below) lead us to believe that $r_{total} < K_m$.

k_v – We estimated k_v for our cells by calculating the relative change in cytosolic and nuclear intensities of the reporter between two conditions. By mass conservation, we know that

$$r_{c,1} + \frac{r_{n,1}}{k_v} = r_{c,2} + \frac{r_{n,2}}{k_v}$$

where $r_{c,i}$ and $r_{n,i}$ are the cytosolic and nuclear concentrations of the reporter in condition i. We then solve for k_v to obtain:

$$k_v = \frac{r_{n,2} - r_{n,1}}{r_{c,1} - r_{c,2}}$$

We make the standard assumption that fluorescence intensity after background subtraction is proportional to concentration. The two conditions we used were anisomycin followed by the addition of JNK inhibitor, which creates the greatest change in nuclear and cytosolic intensities. The model is not sensitive to small variation in k_v. Therefore, to simplify later analysis, we estimated k_v for each cell exposed to those two conditions, and used the average across all cells as the value in the model.

k_{iu}, k_{eu}, k_{ip}, k_{ep} – To estimate the import and export rate constants, we first assumed that the JNK KTR AA mutant approximates the unphosphorylated wild-type JNK KTR, and that the JNK KTR EE mutant approximates the phosphorylated wild-type JNK KTR. This means JNK KTR AA data can be used to determine k_{iu} and k_{eu}, and JNK KTR EE can be used to determine k_{ip} and k_{ep}. Because the mutants cannot be phosphorylated or dephosphorylated, the model for each mutant reduces to a two-state system with two rate constants.

$$\frac{dr_c}{dt} = -k_i \cdot r_c + k_e \cdot r_n$$

$$\frac{dr_n}{dt} = k_v \cdot k_i \cdot r_c + k_v \cdot k_e \cdot r_n$$

The steady state for the system is

$$\frac{r_c}{r_n} = \frac{k_e}{k_i}$$

We treated cells expressing one or the other of these mutant JNK KTRs with leptomycin B (LMB), an inhibitor of nuclear export. If LMB takes effect instantly (or at least very fast compared to k_e and k_i), the system should exponentially approach a new steady state. This is what we experimentally observe (Figure S5A). If LMB inhibits nuclear export by a factor h, where $h = 0$ means complete inhibition and $h = 1$ means no inhibition, then the system after addition of LMB is described by the equations

$$\frac{dr_c}{dt} = -k_i \cdot r_c + h \cdot k_e \cdot r_n$$

$$\frac{dr_n}{dt} = k_v \cdot k_i \cdot r_c + k_v \cdot h \cdot k_e \cdot r_n$$

The new steady state is

$$\frac{r_c}{r_n} = \frac{h \cdot k_e}{k_i}$$

All together, we now have three parameters: k_e, k_i, and h. There are also three parameters in the dynamics of the ratio of cytosolic intensity to nuclear intensity (C/N ratio) of the JNK KTR mutant before and after addition of LMB: the initial steady state, the final steady state, and the timescale of approach to the final steady state. Therefore, for each individual cell expressing one of the

JNK KTR mutants, we were able to uniquely fit k_e, k_i, and h. We used the average values of k_e and k_i for JNK KTR AA as the default values of k_{eu} and k_{iu}, and the average values of k_e and k_i for JNK KTR EE as the default values of k_{ep} and k_{ip}. At the concentration of LMB that we used, the average value of h was about 0.25. We find that, for each mutant, a cell's k_e and k_i are strongly correlated (Figure S5B). The values for the rate constants that are shown in the table above are the means over all cells. In addition, the distribution of

$$\frac{\frac{k_e}{k_i}}{E\left(\frac{k_e}{k_i}\right)}$$

for each non-phosphorylatable JNK KTR mutant (AA, AE, EA, and EE), where $E(k_e/k_i)$ is the mean over all cells for that mutant, is well described by the same log-normal distribution, namely one with $\mu = -0.02$ and $\sigma = 0.22$ (which has a mean of 1 and standard deviation of 0.22) (Figures S5B and S5C).

Based on these results, we conclude that there is considerable cell-to-cell variability in nuclear import and export rates. This variability in import and export creates variability in the localization of any KTR. Supporting this hypothesis, in cells expressing two different JNK KTR mutants (EA and AE), the C/N ratio of the two mutants is strongly correlated (Figure S5E). Interestingly, the C/N ratio of the wild-type JNK KTR shows considerably more cell-to-cell variation ($CV = 0.34$) than any of the JNK KTR mutants, and cells expressing both wild-type JNK KTR and JNK KTR AE show only a weak correlation in the two C/N ratios (Figure S5D). We attribute the additional variability in the baseline C/N ratio of the wild-type JNK KTR to variability in baseline JNK activity.

k_{cat}, K_m – The kinetic parameters for phosphorylation of the reporter by the kinase are the most difficult to constrain using our experimental data. We lack a way to measure absolute concentrations of kinase in live cells. Furthermore, the parameters for phosphorylation are redundant with the concentration of active kinase. Therefore, we relied on work by others (Ember et al., 2008; Figuera-Losada and LoGrasso, 2012; Niu et al., 2007). These authors performed biochemical experiments of JNK with its substrate Atf2 or Jun, and obtained values for the k_{cat} and K_m.

k_{dc}, k_{dn}, K_{md} – We estimated the dephosphorylation parameters by treating cells expressing the wild-type JNK KTR with anisomycin, then with JNK inhibitor. This experimental protocol allows us to get the JNK KTR to a high C/N ratio, then fit the C/N ratio's decay upon addition of inhibitor. Similarly to the experiments with LMB, we assumed the inhibitor takes effect instantly and that the level of inhibition can vary from cell to cell. We also assumed that k_{dc} and k_{dn}, the maximum dephosphorylation rates in the cytosol and the nucleus, are equal. For these fitting procedures, we used the average values of the import and export rate constants. Thus, the only unknown model parameters were k_{dc} and K_{md}. For each individual cell, we ran an optimization problem to find the values of k_{dc} and K_{md} that produced a theoretical time-course of the C/N ratio that most closely matched the observed JNK KTR dynamics after addition of JNK inhibitor. Note that in the model, the C/N ratio is calculated as

$$r_{c/n} = \frac{r_{cu} + r_{cp}}{r_{nu} + r_{np}}$$

Although we were able to produce very close fits in almost all cells, we found that the fitted value of k_{dc} was too low to reproduce the decay (that follows the rise) in the C/N ratio that occurs upon stimulation with physiological inputs (TNF-α, IL-1β, and LPS). More concretely, upon stimulation with any of these molecules, after the C/N ratio peaks, it goes back down faster than our fitted value of k_{dc} would allow. Consequently, we had to double the value of k_{dc} and k_{dn} in order to make the model consistent with experimental data from those physiological stimuli. This adjustment suggests that our assumption that JNK inhibitor instantly inhibits JNK in cells exposed to anisomycin was likely not valid, and that our experimental conditions and fitting procedures can therefore only provide lower bounds for rate constants.

Finally, it is impossible for us to experimentally distinguish between variability in kinase activity and variability in KTR-relevant phosphatase activity. Following the convention of prior computational models of MAP kinase pathways (Mettetal et al., 2008), we have assumed that phosphatase activity (affecting the KTR, not the kinase) is not regulated on the timescale of our experiments. Thus, we assume that the C/N ratio of the KTR is influenced by variability in import/export and by levels of kinase activity, with a level of phosphatase activity that is constant and identical between cells.

Procedure for Estimating Dynamics of the Kinase

Given the dynamics of the KTR that we observe in a particular cell, we would like to use the mathematical model to infer the time-course of active kinase concentration in that cell. This is a difficult inverse problem, because our model is non-linear and our primary observable (the C/N ratio) is a ratio of sums of species in the model. We made the problem tractable for nonlinear optimization by making some simplifying assumptions. Although we can never know for certain what the kinase dynamics actually were, we can say that if the optimization works, then our solution for the kinase dynamics is reasonable.

The most important step in this process is assuming that the dynamics of kinase activity can be approximated by a relatively simple temporal profile, one that can be described using only a few parameters. Here, we focus on the response of JNK to IL-1β. Because the C/N ratio of the JNK KTR in response to IL-1β typically shows a single peak (Figures 4C and 4E), we fit the time-course of active JNK to a trapezoidal form (Figure S5F). In fact, we limit ourselves to only fitting that first peak for each cell (Figures 4D and S5).

Furthermore, based on our immunofluorescence data of phospho-JNK (Figures 2C and S3E), we assume that concentrations of active kinase in cytosol and in nucleus are equal. Importantly, however, the model indicates that KTR technology will still work, even if the kinase is completely nuclear or completely cytosolic (Figures S5K and S5L).

The trapezoidal form for active kinase is flexible, as depending on the values of $T2$ and $T4$, it can look like a square input, or it can increase or decrease gradually. Here, we are being agnostic to the biological processes that produce active JNK. With an existing computational model for a given signaling pathway, it would be possible to fit parameters of the signaling model in the same way that we fit the parameters of the trapezoid.

Importantly, the JNK KTR does not saturate in response to physiological stimuli, i.e., the fraction of reporter that is phosphorylated is always less than 1. Because levels of active JNK induced by IL-1β do not push the JNK KTR above its sensitive range, there is a one-to-one relationship between steady state C/N ratio and active kinase (Figures 4B and S2A). In contrast, anisomycin can apparently saturate the JNK KTR, which we know because the C/N ratio of the JNK KTR increases to the C/N ratio of the JNK KTR EE mutant. This means that we could only estimate a lower bound for active kinase concentration induced by anisomycin. Using the parameterized model, we can also approximate the quantity mentioned earlier for determining the validity of Briggs-Haldane kinetics:

$$\frac{E_0}{K_m + S_0} \cong \frac{0.1}{3 + 0.4} = 0.029 \ll 1$$

As mentioned earlier, cell-to-cell variation in import and export rates affects the C/N ratio of any KTR. To help distinguish variability in import and export from variability in levels of active kinase in individual cells, we created cells expressing both the wild-type JNK KTR and the JNK KTR AE mutant. We use the C/N ratio of the JNK KTR AE mutant in a couple ways. First, for each cell, we calculate a quantity q, where

$$q = \frac{r_{c/n,\ AE}}{E\left(r_{c/n,\ AE}\right)}$$

which is the noise factor in export/import for that cell. We calculate $r_{c/n,\ AE}$ for each cell as the average over the entire time-course, hence we assume that q does not change on the timescale of our experiments. We use q to adjust the import and export rate constants for that cell. In the following notation, $\overline{k_{iu}}$ is the average value of the parameter that we obtained from experiments with leptomycin B, as described earlier.

$$k_{iu} = \frac{\overline{k_{iu}}}{\sqrt{q}}$$

$$k_{ip} = \frac{\overline{k_{ip}}}{\sqrt{q}}$$

$$k_{eu} = \overline{k_{eu}} \cdot \sqrt{q}$$

$$k_{ep} = \overline{k_{ep}} \cdot \sqrt{q}$$

Even with the JNK KTR AE mutant, we cannot distinguish increased import from decreased export, so we distribute the variation equally between the two, which is consistent with our data as shown in Figure S5B.

We perform one other adjustment using the JNK KTR AE mutant, which is that we try to correct for variability in our image analysis by applying a correction factor to the C/N ratio of the wild-type JNK KTR.

$$r_{c/n,\ wt\ corr}(t) = r_{c/n,\ wt}(t) \cdot \frac{E\left(r_{c/n,\ AE}\right)}{r_{c/n,\ AE}(t)}$$

In practice, we have found that this adjustment has very little effect on the results.

At this point, we have adapted the KTR model to our observations for each cell. The last step before running the optimization is to use the properties of each cell's first peak of JNK KTR dynamics to adjust the bounds of the parameters of the trapezoid for active kinase. For example, the upper bound for $T1$ (time of onset of active kinase) is set to 5 minutes plus the time of onset of the first peak. In addition, we explicitly require that $C2$ not be less than either $C1$ or $C3$, i.e., we force active kinase to increase, then decrease. As mentioned previously, only the first peak is fit, which meaning $r_{c/n,\ wt\ corr}(t)$ from the start of the time-course until 20 minutes after the end of the first peak. We have observed that setting these bounds on a cell-by-cell basis considerably improves the fits.

Now we run the optimization, using an extension of the Matlab function fminsearch that accepts general inequality constraints (http://www.mathworks.com/matlabcentral/fileexchange/8277-fminsearchbnd-fminsearchcon). Putting everything together, the optimization can be stated as follows:

Given the $r_{c/n,\ wt\ corr}(t)$ for this cell, our adjusted KTR model for this cell, the trapezoidal profile of the kinase dynamics that we assume, and the bounds we have set for the kinase parameters, what are the parameter values of active kinase that, when plugged into the KTR model, produce a curve for $r_{c/n}(t)$ that best fits (in the least-squares sense) our observed $r_{c/n,\ wt\ corr}(t)$?

In addition to our results shown in Figure 4, the distributions of the parameters that we estimate for active kinase are shown in Figures S5G and S5H.

Regardless of how well the resulting solution fits the data, the solutions from the optimization provide only an estimate of what the dynamics of active JNK in our cells could have been. Therefore, we tested the robustness of our optimization procedure by performing another "round trip" of optimization. First, we used our estimates of kinase dynamics to generate curves of $r_{c/n}(t)$, to which we then added white Gaussian noise of an amplitude comparable to what we observe experimentally. We ran those simulated, noisy dynamics of the JNK KTR back through the optimization procedure, and compared the output kinase dynamics with those that we originally calculated (Figures S5I and S5J). Overall, we observe a strong correlation between input and output, supporting the robustness of our fitting procedure.

Ideally, we would also evaluate our estimates of kinase dynamics, particularly our estimates of active JNK concentration, against existing experimental data. Unfortunately, we know of no published work in which the absolute concentration of active JNK in living cells has been measured. Nevertheless, our estimates of active kinase are consistent with the limited data that are available. Currently there is no available data on the number of JNK1 molecules per NIH 3T3 cell, but p38α, the other MAP kinase that plays a very similar role in cellular signaling, has been estimated at about 100 nM (Schwanhäusser et al., 2011). According to the model, 100 nM of active JNK is roughly the point at which the JNK KTR begins to saturate (Figure 4B). Interestingly, our analysis indicates that most of the cell-to-cell variation observed with respect to JNK activity dynamics is explained by variation in the downregulation of the pathway (Figure S5H).

One possible criticism against KTR technology is the impact of kinase localization in the reporter dynamics. In order to address this question we explored this possibility theoretically using our model. Our results show that a completely biased localization of the kinase toward one compartment (nucleus or cytoplasm) would just slightly shift the response time and the relation between ratio and active kinase concentration (Figures S5K and S5L). Although characterization should be performed on a case-by-case basis, this observation suggests that the fast nucleocytoplasmic shuttling dynamics of the reporters allow KTR technology to be used even when kinase localization is biased.

SUPPLEMENTAL REFERENCES

Edelstein, A., Amodaj, N., Hoover, K., Vale, R., and Stuurman, N. (2010). Computer control of microscopes using microManager. Curr. Protoc. Mol. Biol. *92*, 14.20.1–14.20.17.

Ember, B., Kamenecka, T., and LoGrasso, P. (2008). Kinetic mechanism and inhibitor characterization for c-jun-N-terminal kinase 3alpha1. Biochemistry *47*, 3076–3084.

Feige, J.N., Sage, D., Wahli, W., Desvergne, B., and Gelman, L. (2005). PixFRET, an ImageJ plug-in for FRET calculation that can accommodate variations in spectral bleed-throughs. Microsc. Res. Tech. *68*, 51–58.

Figuera-Losada, M., and LoGrasso, P.V. (2012). Enzyme kinetics and interaction studies for human JNK1β1 and substrates activating transcription factor 2 (ATF2) and c-Jun N-terminal kinase (c-Jun). J. Biol. Chem. *287*, 13291–13302.

Kamentsky, L., Jones, T.R., Fraser, A., Bray, M.A., Logan, D.J., Madden, K.L., Ljosa, V., Rueden, C., Eliceiri, K.W., and Carpenter, A.E. (2011). Improved structure, function and compatibility for CellProfiler: modular high-throughput image analysis software. Bioinformatics *27*, 1179–1180.

Kosugi, S., Hasebe, M., Tomita, M., and Yanagawa, H. (2008). Nuclear export signal consensus sequences defined using a localization-based yeast selection system. Traffic *9*, 2053–2062.

Kosugi, S., Hasebe, M., Matsumura, N., Takashima, H., Miyamoto-Sato, E., Tomita, M., and Yanagawa, H. (2009). Six classes of nuclear localization signals specific to different binding grooves of importin alpha. J. Biol. Chem. *284*, 478–485.

Niu, L., Chang, K.C., Wilson, S., Tran, P., Zuo, F., and Swinney, D.C. (2007). Kinetic characterization of human JNK2alpha2 reaction mechanism using substrate competitive inhibitors. Biochemistry *46*, 4775–4784.

Schwanhäusser, B., Busse, D., Li, N., Dittmar, G., Schuchhardt, J., Wolf, J., Chen, W., and Selbach, M. (2011). Global quantification of mammalian gene expression control. Nature *473*, 337–342.

Segel, A.L., and Slemrod, M. (1989). The quasi-steady-state assumption: a case study in perturbation. SIAM Rev. *31*, 446–477.

Wen, W., Meinkoth, J.L., Tsien, R.Y., and Taylor, S.S. (1995). Identification of a signal for rapid export of proteins from the nucleus. Cell *82*, 463–473.

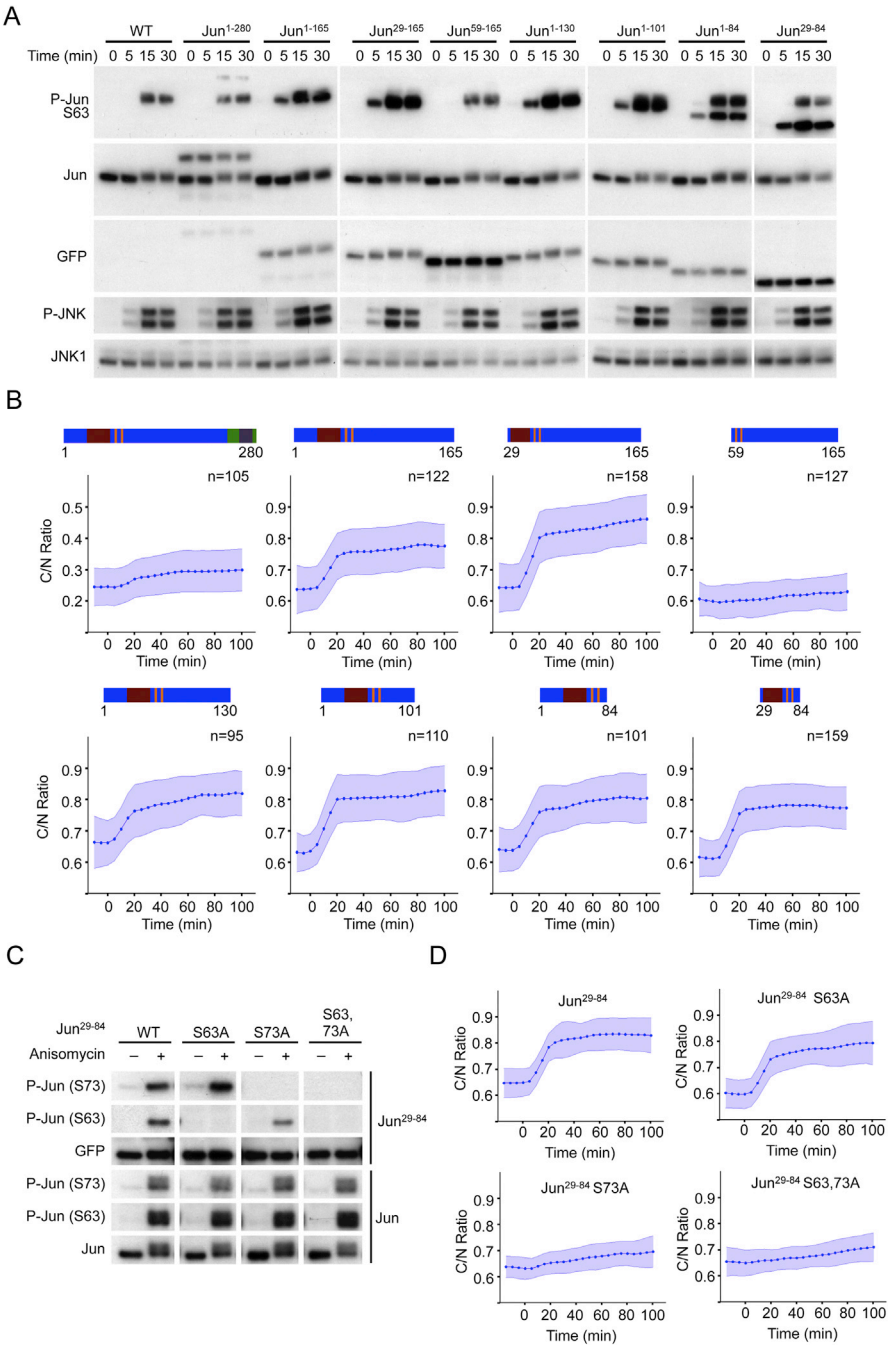

Figure S1. c-Jun Fragment Analysis, Related to Figure 1

(A) 3T3 cells (wild-type or expressing indicated c-Jun fragments fused to Clover) were stimulated with anisomycin (50 ng/ml) and harvested at indicated time points for Western Blot analysis. Representative of 2 independent experiments.

(B) Cell lines used in Panel a were stimulated with anisomycin (50 ng/ml), imaged and quantified as described in Methods. Schematic representation of each fragment is shown for clarity. Data represent the mean ± SD from the indicated number of cells obtained from 2 independent experiments.

(C) 3T3 cells (wild-type or expressing indicated c-Jun$^{29–84}$ mutants) were stimulated with anisomycin (50 ng/ml) and harvested at indicated time points for Western Blot analysis. Representative of 2 independent experiments.

(D) Cell lines used in Panel a were stimulated with anisomycin (50 ng/ml), imaged and quantified as described in Methods. Data represent the mean ± SD from more than 100 cells for each mutant obtained from 2 independent experiments.

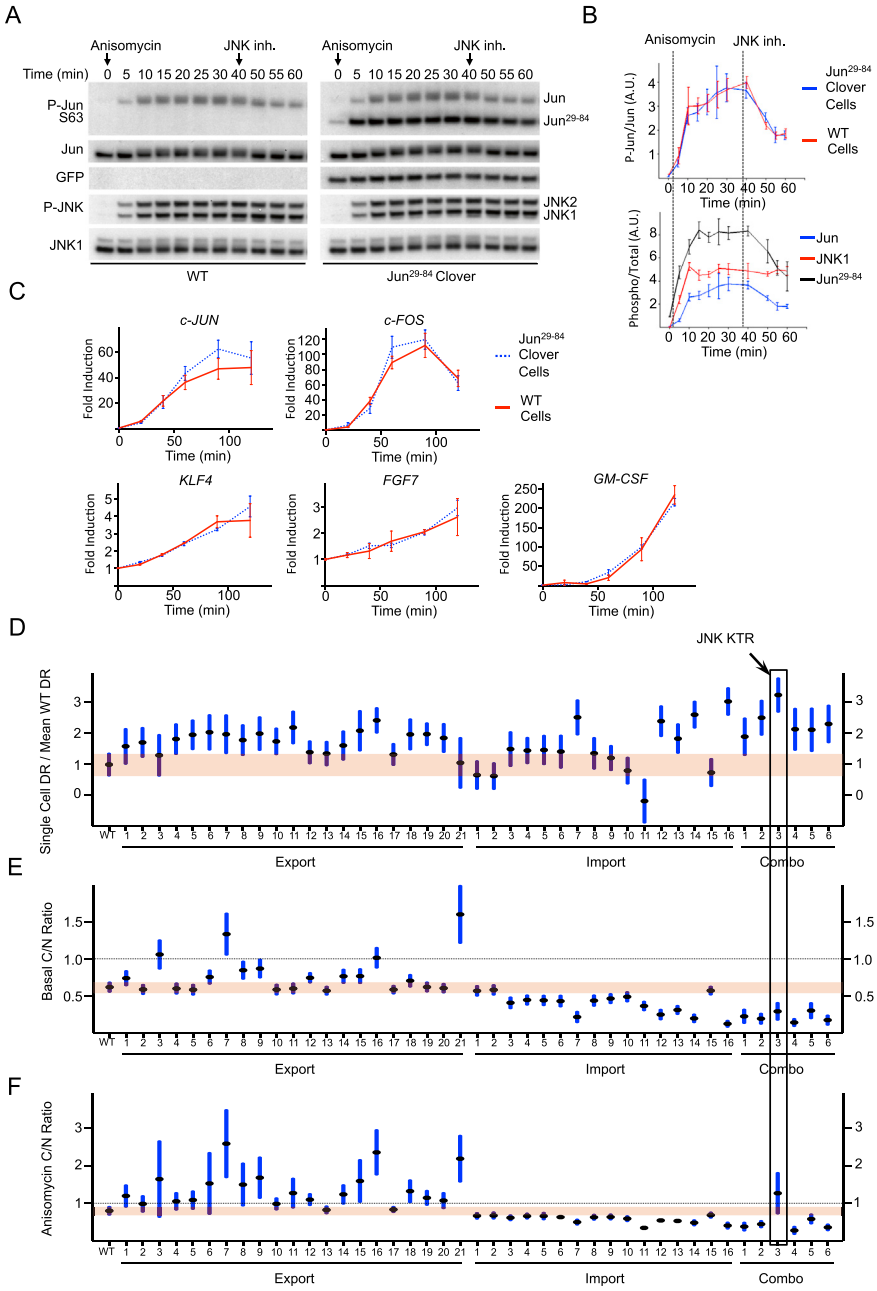

Figure S2. Validation and Optimization of c-Jun$^{29–84}$, Related to Figure 1

(A) 3T3 cells (wild-type or expressing c-Jun$^{29–84}$) were stimulated with anisomycin (50 ng/ml) and harvested at indicated time points for quantitative Western Blot analysis. 10 μM JNK inhibitor VIII was added when indicated. Representative of 3 independent experiments.

(B) Quantification of endogenous c-Jun phosphorylation from wild-type or c-Jun$^{29–84}$ samples in Panel a (Upper panel). Quantification of phosphorylated over total c-Jun, c-Jun$^{29–84}$ and JNK1 proteins from c-Jun$^{29–84}$ samples in Panel a (Lower panel). Data represent the mean ± SD from 3 independent experiments.

(C) 3T3 cells (wild-type or expressing c-Jun$^{29–84}$) were stimulated with anisomycin (50 ng/ml) and harvested at indicated time points for quantitative PCR gene expression analysis. Indicated genes were measured as a representation of c-Jun dependent genes.

(D) Data presented in Figure 1D are shown for comparison.

(E and F) Basal (E) and anisomycin treated (F) cytoplasmic over nuclear ratio for engineered variants shown in Figure 1C. Dashed line indicates the boundary between cytoplasmic (above) and nuclear (below) localizations. Data represent the mean ± SD from more than 50 cells for each variant, obtained from 2 independent experiments.

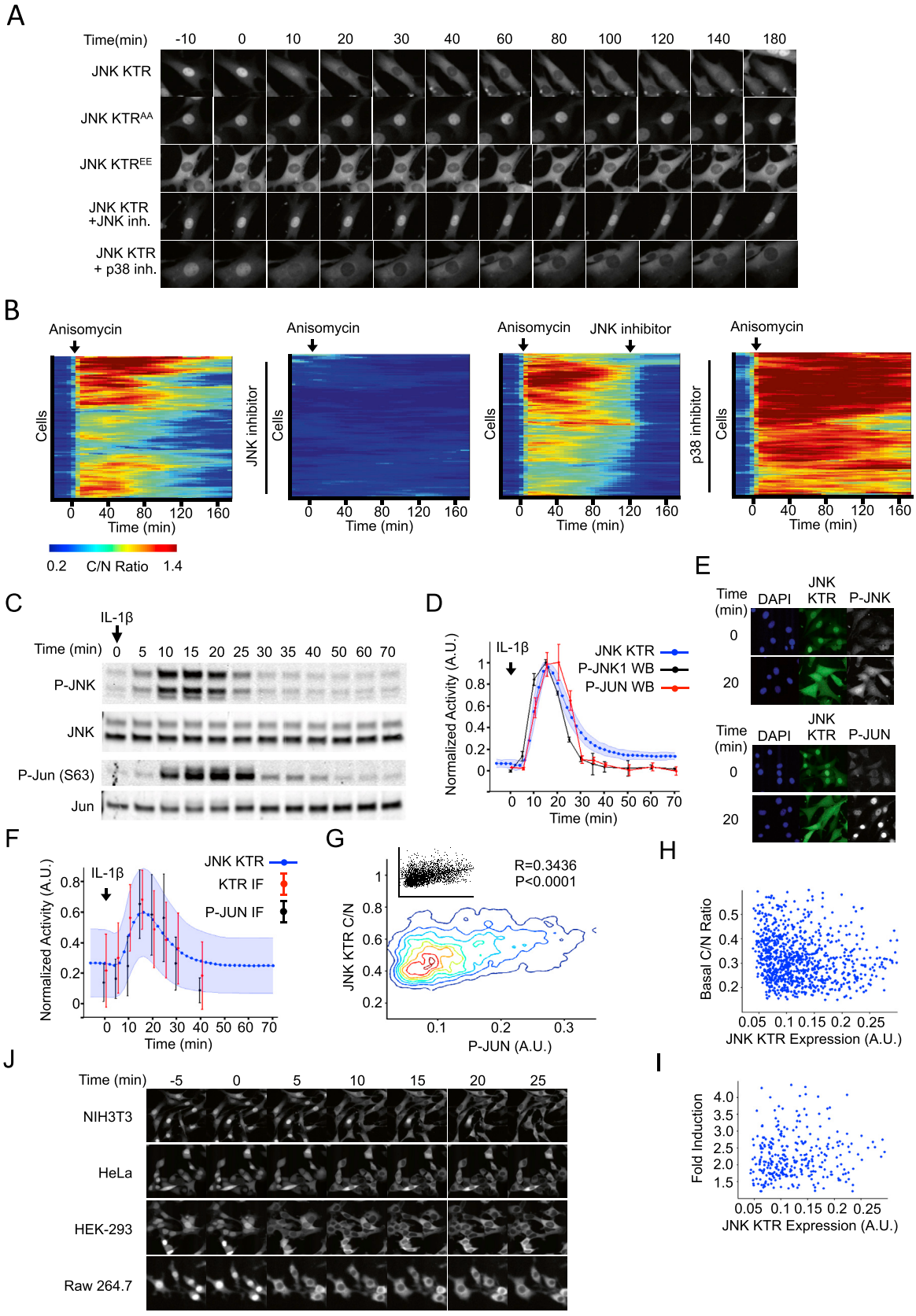

(legend on next page)

Figure S3. JNK KTR Enables Single-Cell Measurements of Kinase Activity Dynamics, Related to Figure 2

(A) 3T3 cells expressing JNK KTR (wild-type or with phospho sites mutated to alanine, AA, or glutamic, EE) were stimulated with anisomycin (50 ng/ml) and imaged at indicated time points. Where indicated (+ JNK inh. or + p38 inh.), cells were preincubated for 45 min with 10 μM JNK inhibitor VIII or 10 μM SB203580. Representative cells are shown for each construct or condition over time.

(B) Heat maps of data presented in Figure 1G are shown. Data represent more than 100 cells for each condition, obtained from 3 independent experiments.

(C) 3T3 cells were stimulated with IL-1β (1 ng/ml) and harvested at indicated time points for quantitative Western blot (WB) analysis. Representative of 3 independent experiments.

(D) JNK KTR cells were stimulated with IL-1β (1 ng/ml), imaged and quantified as described in Methods. Three independent experiments were performed resulting in 980 single cells measured. KTR data represent the mean ± SD from the 3 experiment means (averaged to mimic in silico WBs). WB data are calculated as the fraction of phosphorylated over total and represents the mean ± SD from 3 independent experiments. All data sets were normalized between 0 and 1 for comparison.

(E) 3T3 JNK KTR cells were stimulated with anisomycin (50 ng/ml) for 0 or 20 min and fixed with 4% PFA for immunofluorescence (IF) analysis. Phospho-JNK (left) and phospho-c-Jun(S63) (right) antibodies were detected using a Cy5-linked secondary antibody. 10 ng/ml of DAPI was used to stain the nucleus. Representative cells are shown for each time point.

(F) 3T3 JNK KTR cells were stimulated with IL-1β (1 ng/ml) for indicated times and fixed with 4% PFA for quantitative IF analysis. 10 images were taken for each time point and quantified as described in Methods. For each cell C/N KTR ratio (red) and phospho-Jun intensity (black) were determined. All data sets were normalized between 0 and 1 for comparison. Data represent the mean ± SD from more than 500 cells for each time point obtained from 2 independent experiments. IF data are overlaid on the dynamic JNK KTR data set (blue). Note that in this case, JNK KTR dynamic data represent the mean ± SD from all individual cells (n = 980), obtained in 3 independent experiments.

(G) IF data obtained in Panel b represented as contour scatter plot. Single cell JNK KTR ratio and phospho-Jun intensity from all time points are shown. Contour color represent areas of increasing data point density. Raw scatter plots fitted to a linear regression are shown together with R and P values.

(H) JNK KTR cells were imaged at a single time point and quantified as described in Methods. Correlations of expression level with basal C/N ratio are shown. Data represent 248 cells obtained from 3 independent experiments.

(I) JNK KTR cells were stimulated with IL-1β (1 ng/ml), imaged and quantified as described in Methods. Peaks were identified using custom software. Correlations between fold ratio induction and expression level are shown. Data represent 92 cells obtained from 2 independent experiments.

(J) Indicated cell lines expressing JNK KTR were stimulated with anisomycin (50 ng/ml) and imaged at indicated time points. Representative cells are shown for each cell line over time.

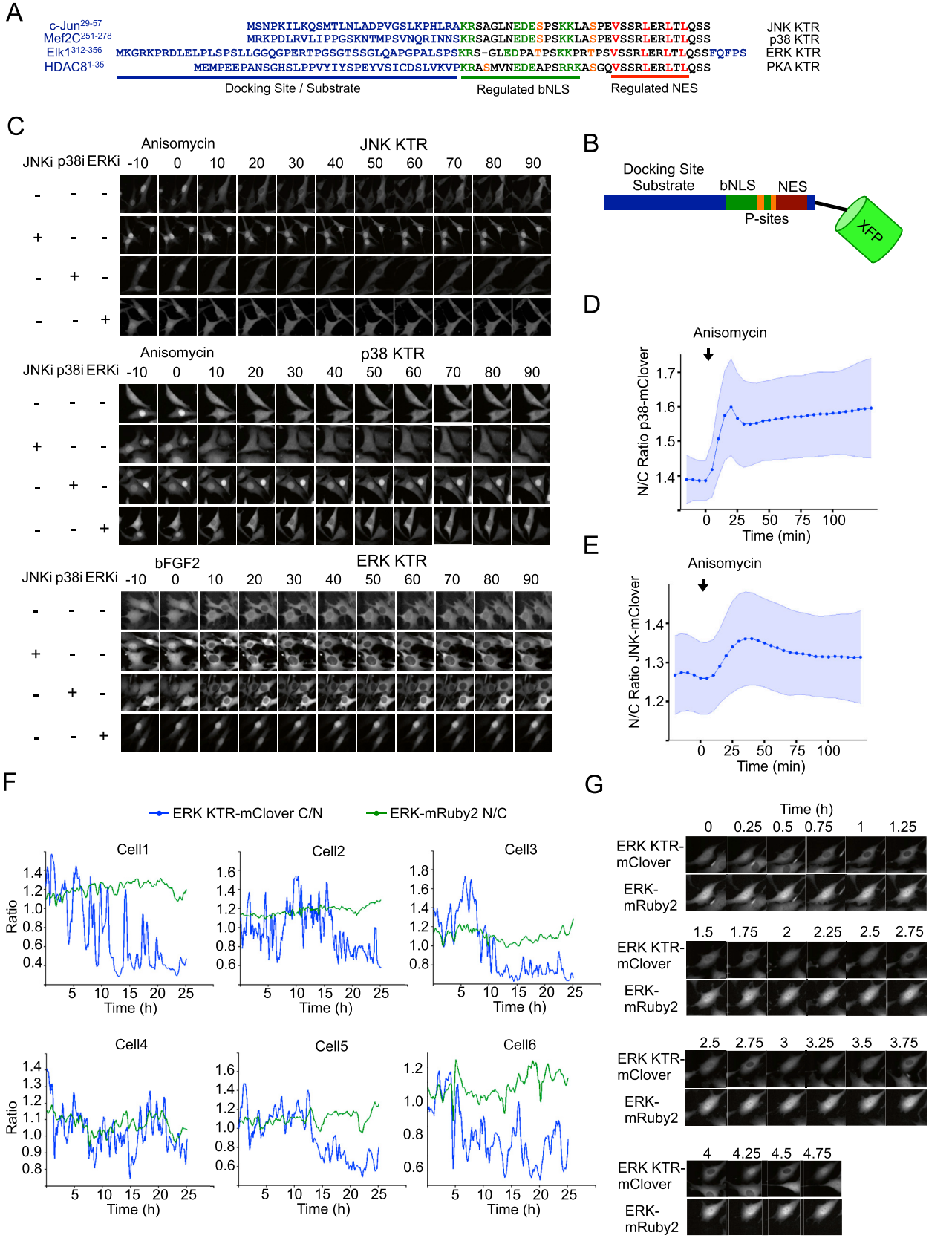

(legend on next page)

Figure S4. KTR Technology Is Generalizable to Other Kinases and Has a Better Dynamic Range than MAPK Localization, Related to Figure 3

(A) Specific sequences used for developing all KTRs shown in this paper. Proteins from which kinase docking site was extracted is specified on the left. Color code matches the schematic representation shown in Panel a.

(B) Schematic representation of KTR design.

(C) Cells expressing MAPK KTRs were stimulated with anisomycin (50 ng/ml) or bFGF2 (100 ng/ml) and imaged at indicated time points. Cells were preincubated for 45 min with 10 μM JNK inhibitor VIII (JNKi), 10 μM SB203580 (p38i) or 100 nM PD032591 (ERKi) as indicated.

(D and E) Cells expressing p38 (D) and JNK (E) fused to mClover were stimulated with anisomycin (50 ng/ml), imaged and quantified as described in Methods (note that N/C ratio is used in this case). Data represent the mean ± SD from more than 100 individual cells, obtained in 2 independent experiments.

(F) Cells expressing ERK KTR-mClover and ERK1-mRuby2 were imaged over time and quantified as described in methods. Localization dynamics of both constructs are shown for 6 representative cells.

(G) Representative pictures of cells treated as in Panel c are shown.

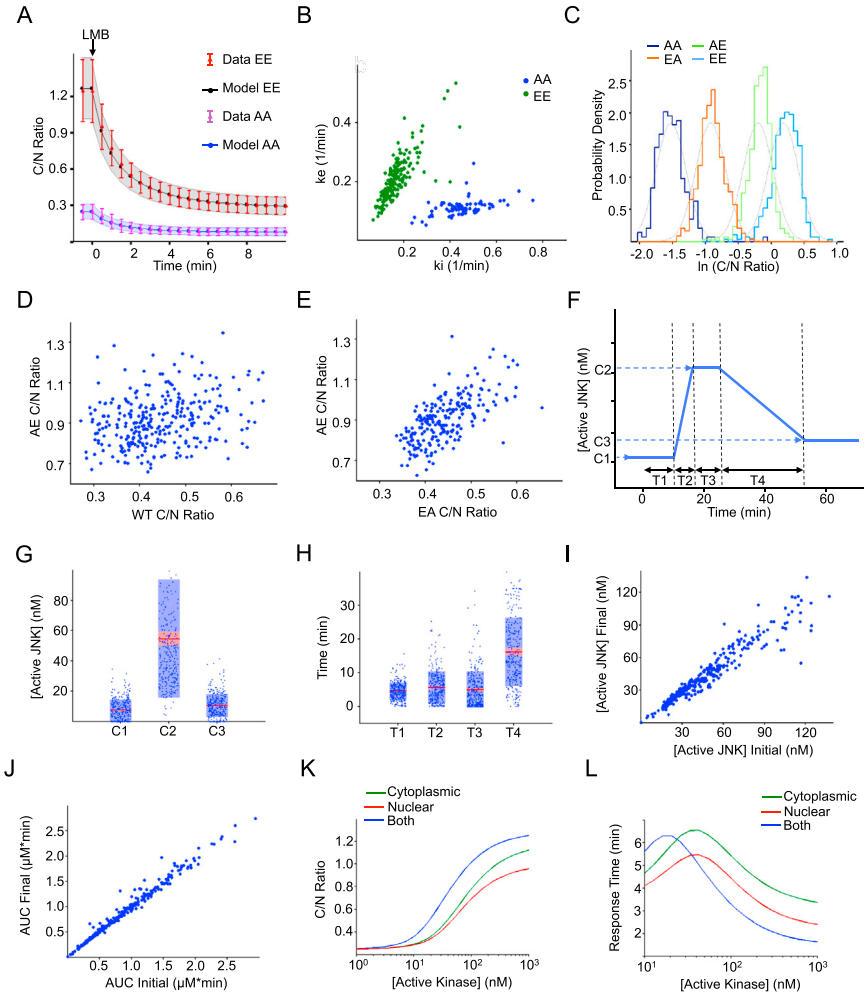

Figure S5. Model Fitting, In-Cell Control Validation, and Results, Related to Figure 4

(A) 3T3 cells expressing JNK KTR nonphosphorylatable (AA) and phosphomimetic (EE) mutants were imaged upon addition of Leptomycin B (50 ng/ml). Images were quantified as descrived in Methods. Data represent the mean ± SD of more than 100 cells (Data) obtained from 3 independent experiments. Data were fitted to the model obtaining rate constants for each individual cell. Mean ± SD of simulated data is shown (Model).

(B) Correlations of estimated import and export rate constants for JNK KTR AA and EE obtained in Panel a.

(C) Cells expressing indicated mutant versions of JNK KTR were imaged and quantified under basal conditions. Histograms of basal C/N ratio are shown. Solid gray lines are probability densities of the same log-normal distribution ($\mu = 0.02$, $\sigma = 0.22$) that has been shifted to fit each mutant.

(D and E) Cells expressing two versions of JNK KTR (wild-type and AE [D] or AE and EA [E]) were imaged at a single time point and quantified as described in Methods. Values of C/N for wild-type and mutant JNK KTRs were obtained. Correlations for each individual cell between mutants AE versus EA (E) and WT versus AE (D) are shown. Data represent more than 100 cells.

(F) Schematic representation of the temporal profile assumed for estimating kinase activity. Four times (T1-T4) and 3 concentrations (C1-C3) were explored to estimate the kinase activity dynamics that generate the observed KTR dynamics.

(G and H) distributions of the parameters shown in Panel b for cells stimulated with 1 ng/ml IL-1β. Individual data points (blue dots), mean (red line), 95% SEM interval (red shadow) and SD (blue shadow) are shown for each parameter. Data represent 302 cells.

(I and J) C/N ratios were obtained from the temporal profiles calculated for Figure 4E (Initial). To test the robustness of our fitting procedure, noised ratio dynamics were then used to recalculate kinase activity temporal profiles (Final). Correlations between initial and final maximum active JNK concentration (I) and area under the curve (AUC) (J) are shown.

(K and L) Model based relationship between steady state C/N ratio (K) or half response time (L) and concentration of active kinase when kinase is localized just in the Cytoplasm (green), Nucleus (red) or Both (blue). JNK KTR parameters were used.

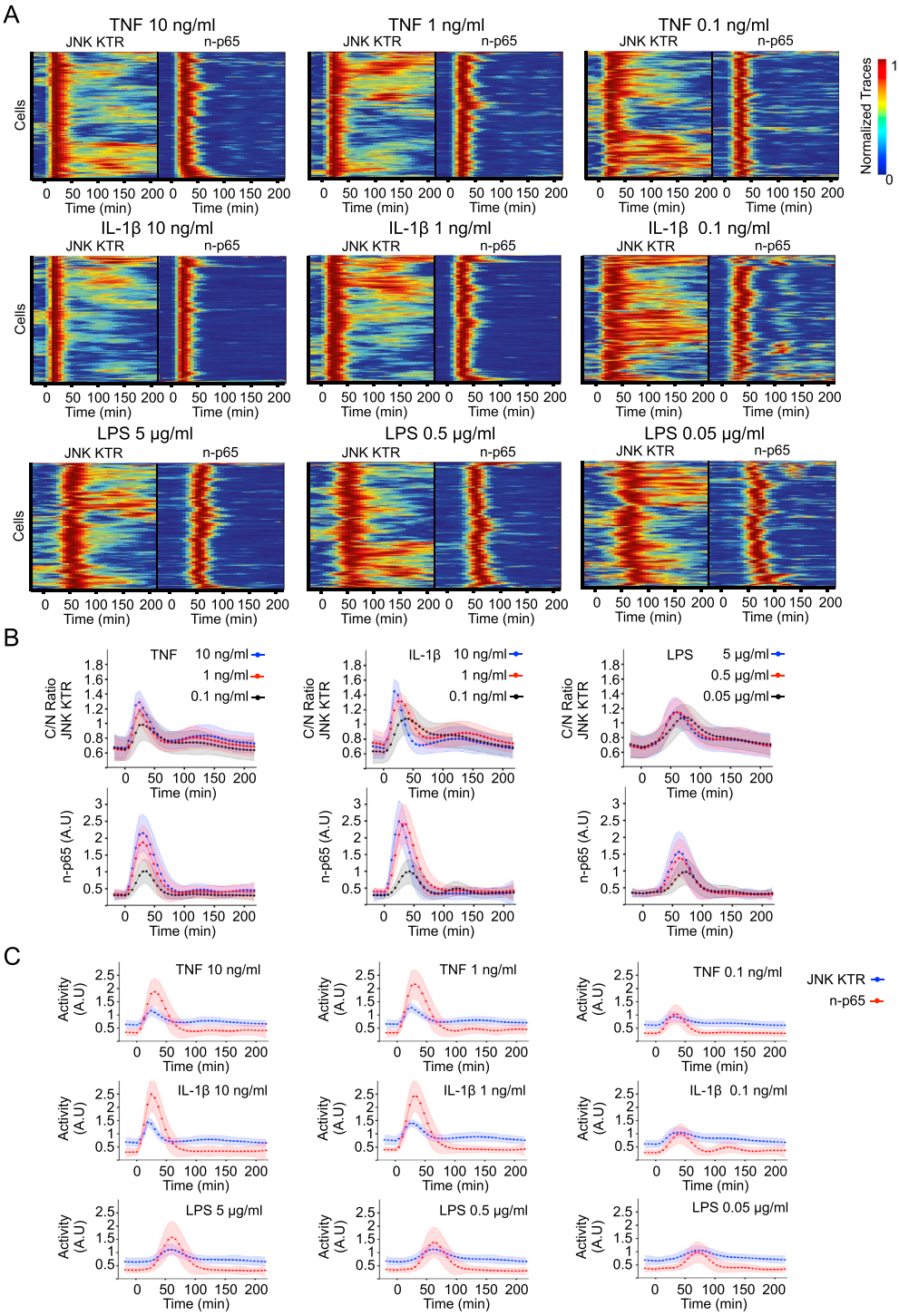

Figure S6. JNK KTR Enables the Measurement of Dynamic JNK Kinase Activity within the Innate Immune Signaling Network, Related to Figure 5

(A) Clonal line 3B8 (*RelA*$^{-/-}$ KO 3T3, H2B-EGFP, p65-DsRed and JNK KTR-mCerulean3) was stimulated with indicated concentrations of TNFα, IL-1β or LPS, imaged and quantified as described in Methods. Heat maps represent clustered individual cells with normalized JNK KTR and nuclear p65 (n-p65) dynamics displayed in tandem. Each condition represents a minimum of 300 cells obtained from 3 independent experiments.

(B and C) Average population dynamics from data obtained for Panel a. Data represent the mean ± SD from more than 300 cells per condition obtained from 3 independent experiments.

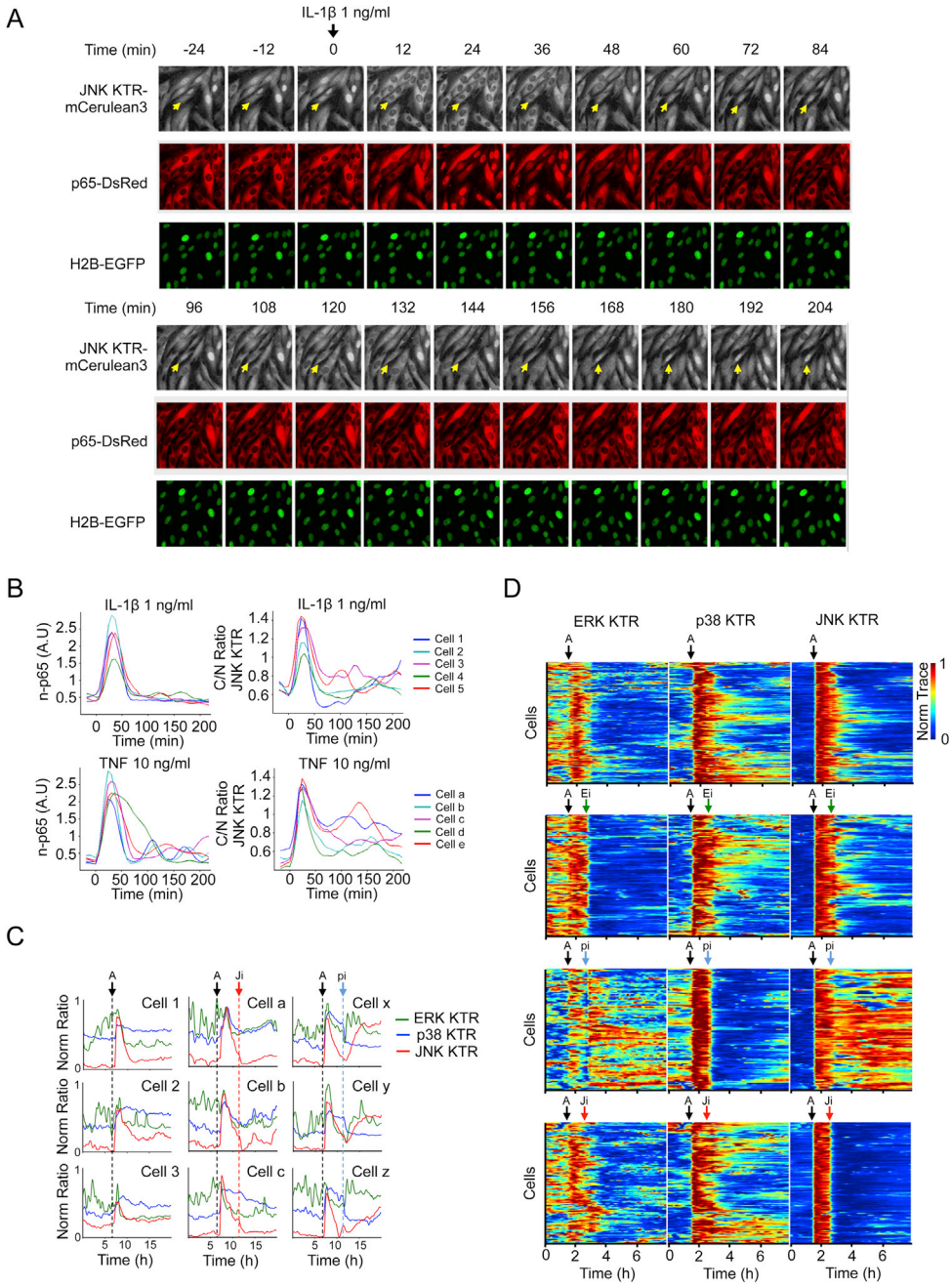

Figure S7. KTR Technology Reveals MAP Kinase Activity Fluctuations, Related to Figure 6

(A) Clonal line 3B8 was stimulated with IL-1β (1 ng/ml) and imaged at indicated time points. A single field of view is shown in the 3 channels. Arrow indicates an oscillating cell.

(B) Clonal Line 3B8 was stimulated with IL-1β (1 ng/ml) or TNF (10 ng/ml), imaged and quantified as described in Methods. 5 single cells are shown in the p65 channel and in the JNK KTR channel. Note Cell 5, a and e as oscillating cells.

(C) Representative traces of cells shown in Figures 6D and 6E.

(D) 4C cell line was stimulated with Anisomycin (A) (50 ng/ml) where indicated (black arrow) and treated with100 nM PD032591 (Ei), 10 μM SB203580 (pi) or 10 μM JNK inhibitor VIII (Ji) (green, blue or red arrows respectively). Images were taken every 8 min and quantified as described in Methods. Heat maps for more than 100 cells are shown.